Supplementary Material

Effects of EVA based compatibilizers/toughers on morphological and mechanical properties of PP/EVA/HNT blend nanocomposites

Salih Doğu, Emre Tekay and Sinan Şen

Department of Polymer Engineering, Yalova University, Yalova, 77200, Turkey

Corresponding author: Sinan Şen

Email: sinans@yalova.edu.tr

SEM Images

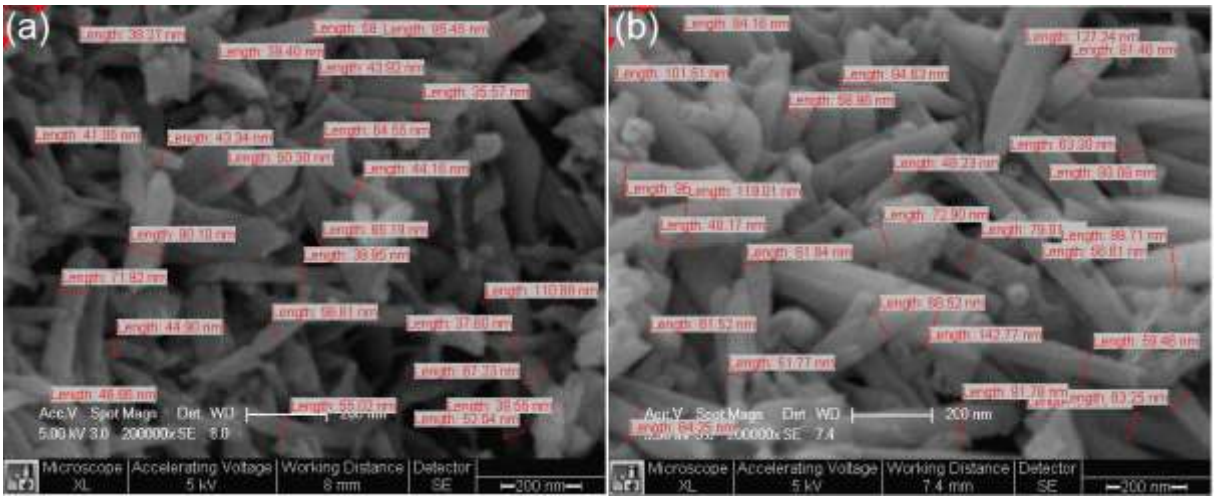

Figure S1. SEM images of (a) HNT and (b) Org-HNT showing nanotube diameters

Particle Size Distribution of Elastomeric Domains

Figure S2-Figure S5 show size distribution of elastomeric domains in PP blends and composites. As it is observed from Figure S2, the number of elastomer particles having larger sizes increases as amount of EVA in the blend increases. The average sizes of the elastomer particles dispersed in the matrix are 205.46 nm, 251.25 nm and 347.48 nm for PP3EVA, PP9EVA and PP15EVA, respectively.

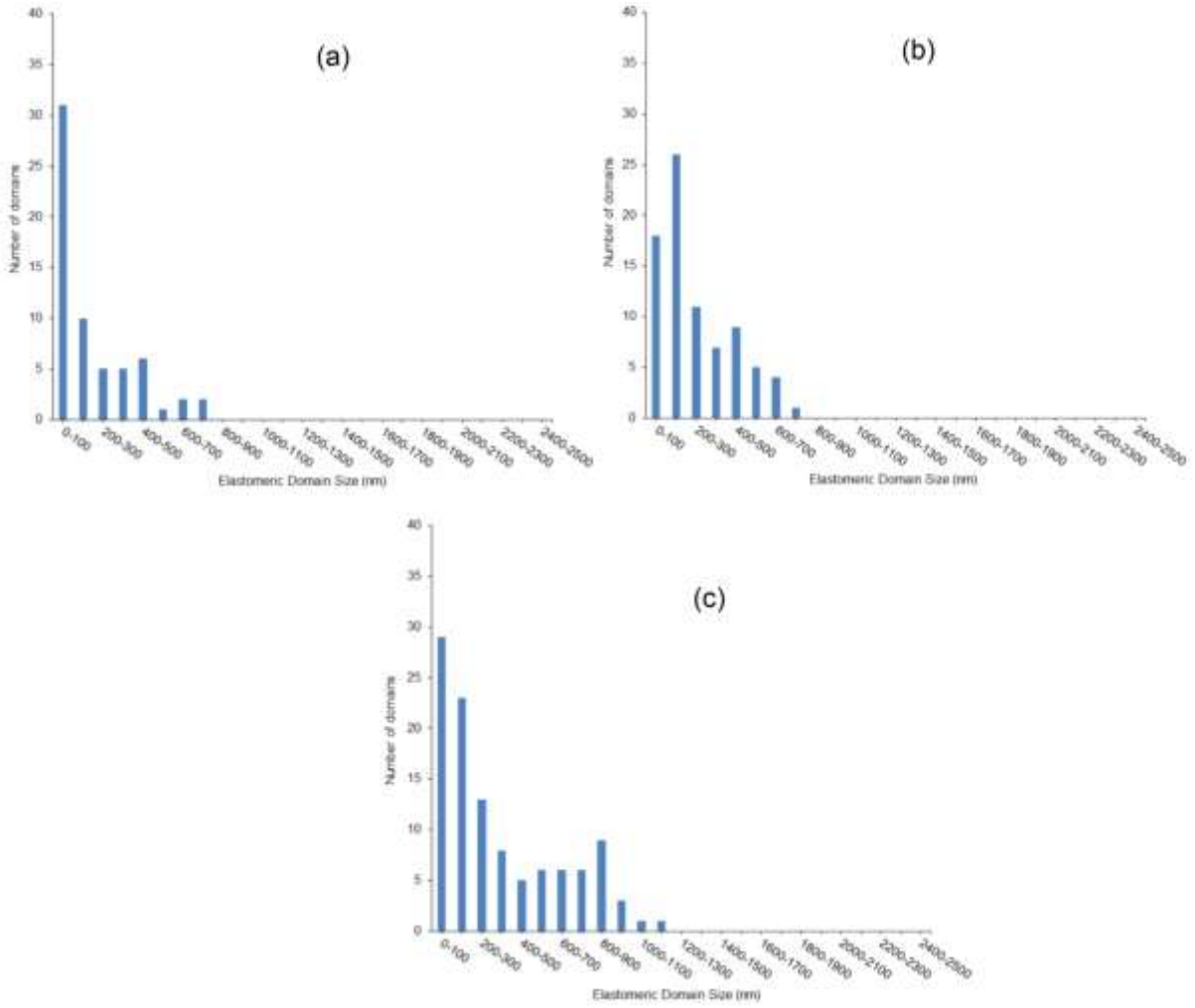

Figure S2. The size distribution of elastomeric domains of (a) PP3EVA, (b) PP9EVA and (c) PP15EVA blends

Figure S3 shows the size distribution for 1 % Org-HNT loaded composites. Compared to PP3EVA blend (Figure S2a), number of small-sized (100-500 nm) elastomer domains were found to be almost 1.5 times higher for EVACO compatibilized composite (1H1ECO(2EVA)) (Figure S3c).

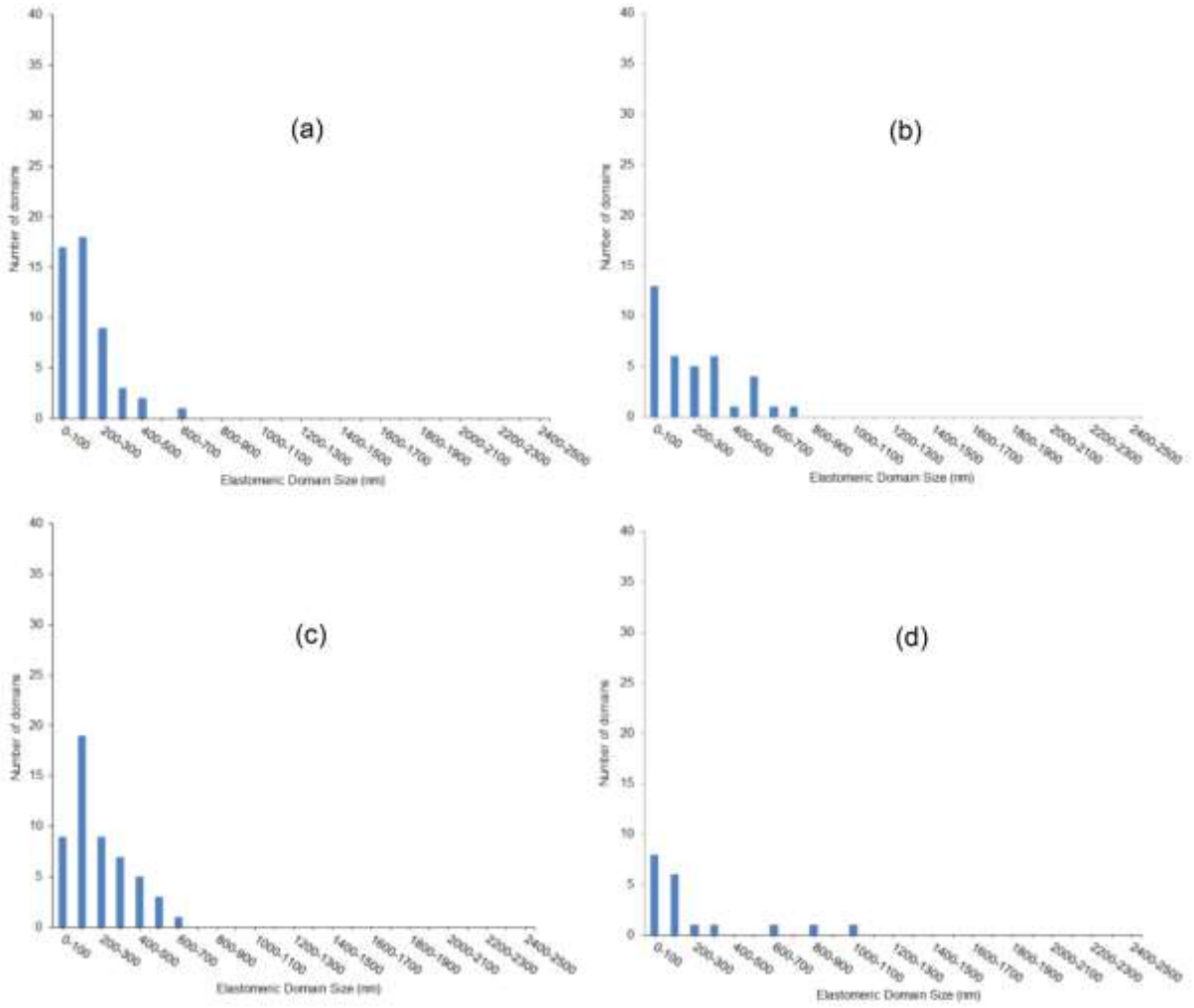

Figure S3. The size distribution of elastomeric domains of (a) 1H3EVA, (b) 1H1EMA(2EVA), (c) 1H1ECO(2EVA) and (d) 1H1PMA(2EVA) composites

All other composites show different size distribution depending on the amount of nanotube and elastomer domain used as well as nanotube location. The formation of larger sized and irregularly-shaped elastomer domains may be due to their coalescence abilities in presence of nanotubes between elastomer particles or around them. [1, 2] It may also be due to clustering of nanoparticle induced clustering of elastomer droplets in which the elastomeric particles keep their elongated shapes during melting process.[1, 2] It is also known that if the clays are present at interphase and inside the elastomeric domains, the average size of elastomeric particles increases.[3] This morphology refinement (from droplet morphology to an irregularly-shaped one) has been ascribed to viscosity increase of elastomeric droplets containing carbon nanotubes as high aspect ratio filler.[4]

In current study, the selective location of nanotubes inside the EVA based compatibilizers and EVA and at their interphases depending on their polarities might result in elastomer phase in different sizes, especially at high loading degrees of the nanotubes and elastomer phase. It is clear from Figure S4 and Figure S5, that only the composites compatibilized with EVA-g-MA and EVACO in 3% and 5 % Org-HNT loadings show the elastomer domains in larger sizes (above 1500 nm). This can be explained with their relatively higher polarities resulting in more interaction with HNT surfaces as compared to EVA and PP-MA, leading to abovementioned probable coalescence or clay bridged clusters as irregularly-shaped morphologies.[1]

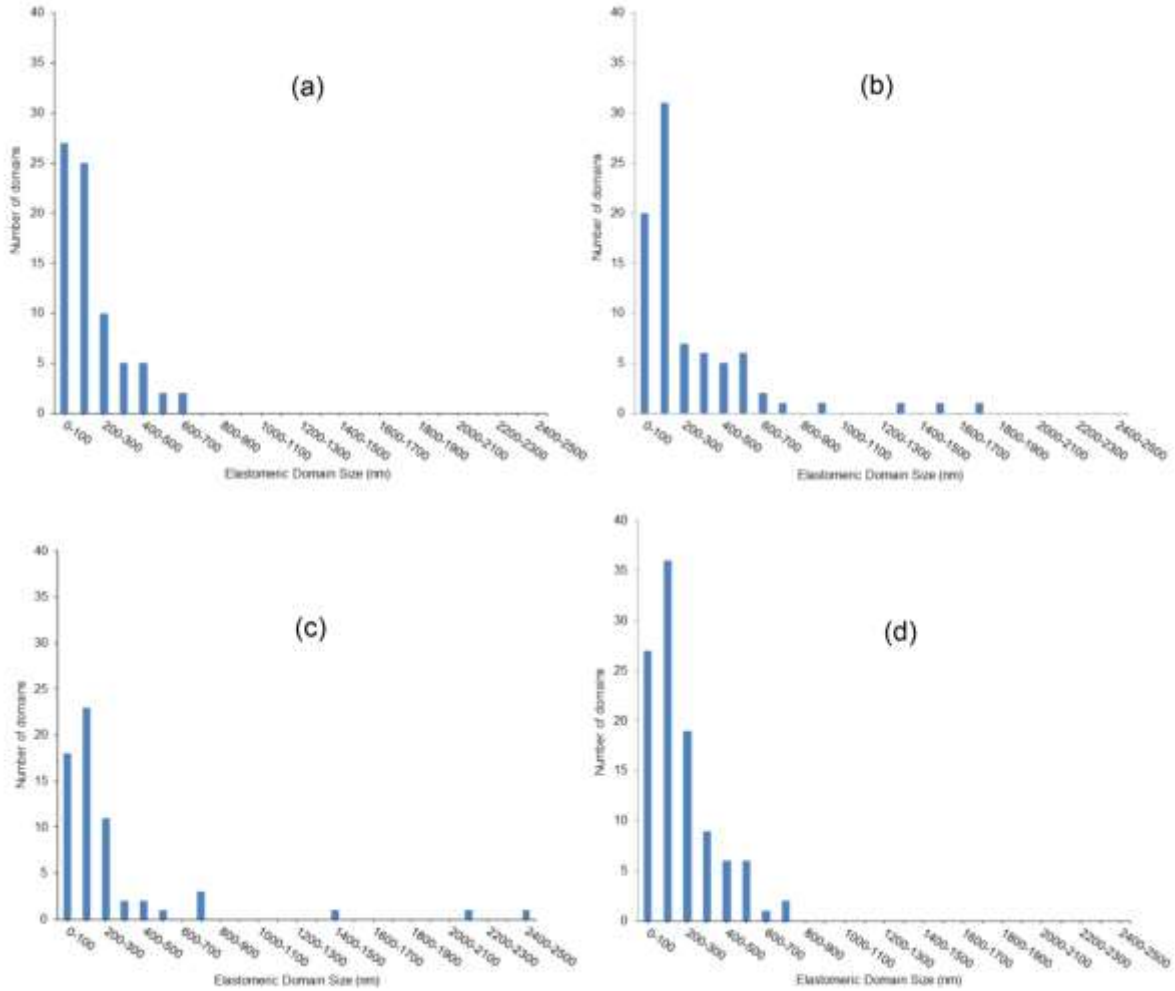

Figure S4. The size distribution of elastomeric domains of (a) 3H9EVA, (b) 3H3EMA(6EVA), (c) 3H3ECO(6EVA) and (d) 3H3PMA(6EVA) composites

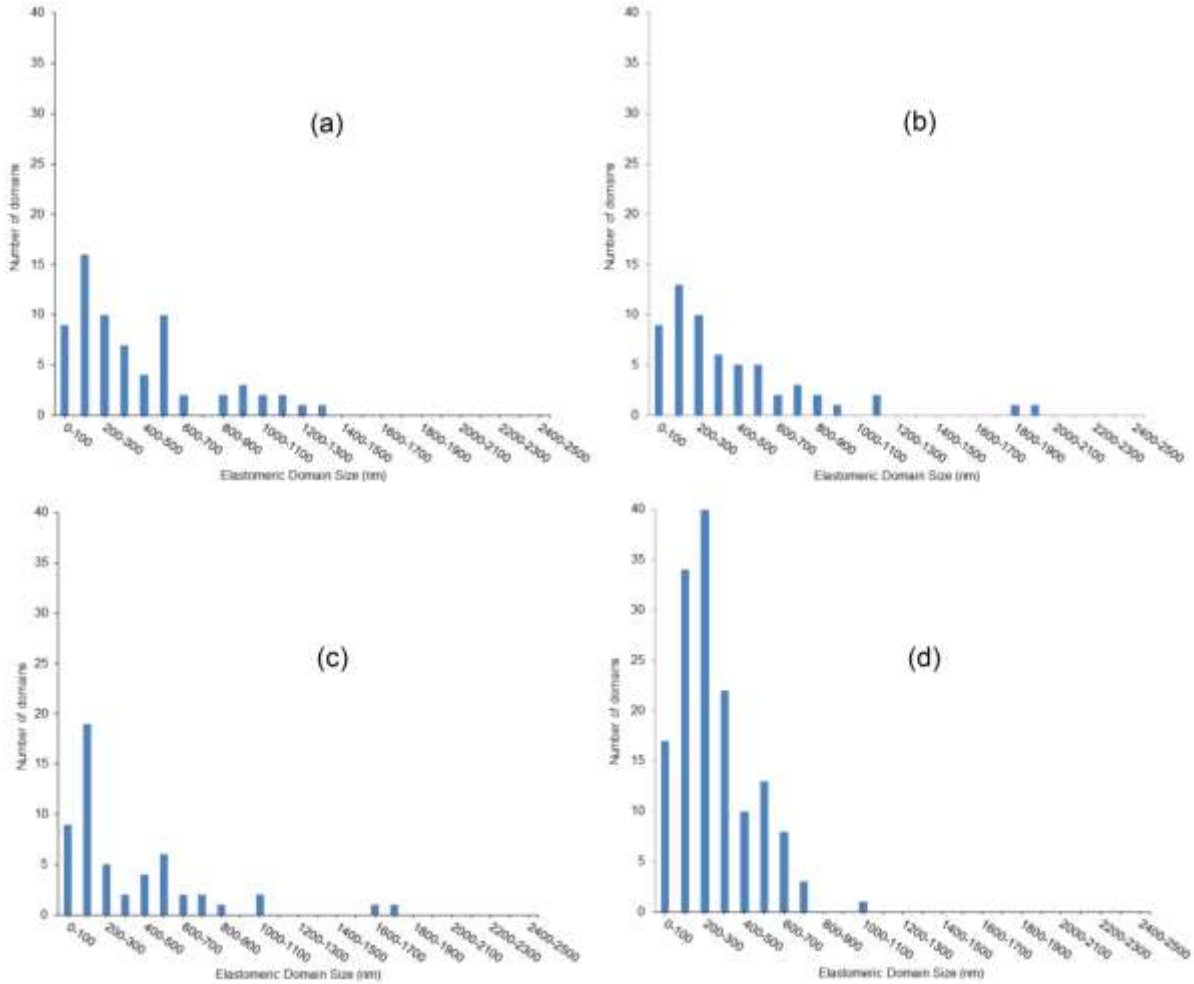

Figure S5. The size distribution of elastomeric domains of (a) 5H15EVA, (b) 5H5EMA(10EVA), (c) 5H5ECO(10EVA) and (d) 5H5PMA(10EVA) composites

FTIR analyses of EVA-g-MA and EVACO polymers

In the FTIR spectra of EVA-g-MA and EVACO (Figure S6), the peaks between 2850 cm^{-1} and 2919 are ascribed to symmetric and asymmetric CH_2 vibrations. The peaks at 1737 cm^{-1} and 1735 cm^{-1} are due to carbonyl stretching of vinyl acetate. The peak at 1712 cm^{-1} is for carbonyl group stretching of carbon monoxide in the backbone of EVACO. The peaks at 1467 and 1373 cm^{-1} in the spectrum of EVACO-g-MA and 1465 and 1372 cm^{-1} in that of EVACO are ascribed to CH scissoring in $–CH_2–$ and symmetric deformation of CH in $–CH_3$, respectively. The peak at 3204 cm^{-1} can be assigned to hydrogen bonded OOH groups[5, 6] and vibrations of adsorbed water molecules since EVA-g-MA has hydrophilic character due to its polar groups. The peaks at 1237 and 1239 (Figure S6) correspond to the twisting and wagging of CH in $–CH_2–$. The peaks at 1020 cm^{-1} and 720 cm^{-1} are due to to C-O-C stretching and the rocking vibration of CH, respectively.[6]

FTIR analyses of Org-HNT and 3H3EMA(6EVA)

FTIR spectra of 3H3EMA(6EVA) as another representative composite sample and Org-HNT were given in Figure S7. The carbonyl (C=O) stretching of vinyl acetate of EVA-g-MA polymer (Figure S6) appeared at 1741cm^{-1} in the spectrum of 3H3EMA(6EVA) nanocomposite (Figure S7). This is due to intermolecular hydrogen bonding between the carbonyl group and hydroxyl groups of Org-HNT.[6] Moreover, the appearance of new bands at 1737 cm^{-1} and 1703 cm^{-1} (Figure S7) can be related to the formation of ester bond between MA group of EVA-g-MA polymer and HNT surface.[7-9] The relatively broad and small peak at 1021 cm^{-1} (Figure S7), representing the C-O-C stretching of vinyl acetate can be due to interaction of EVA-g-MA with OH groups of Org-HNT. The peaks at 905 cm^{-1} and 999 cm^{-1} in the spectrum of Org-HNT was shifted to 899 cm^{-1} and 997 cm^{-1}, respectively. The Si-O stretching peak at 1120 cm^{-1} was also shifted to 1045 cm^{-1} (Figure S7). These changes can be attributed to hydrogen bonding interactions between Org-HNT and EVA-g-MA polymer as mentioned for 3H3ECO(6EVA).[10, 11] The smaller shift observed for absorption of Al-OH (from 3693 cm^{-1} to 3695 cm^{-1}) (Figure S7), on the other hand, can be accepted as an indication of aluminol groups inside the lumen of Org-HNT interacting much less via carbonyl groups of EVA-g-MA polymer.[12-13]

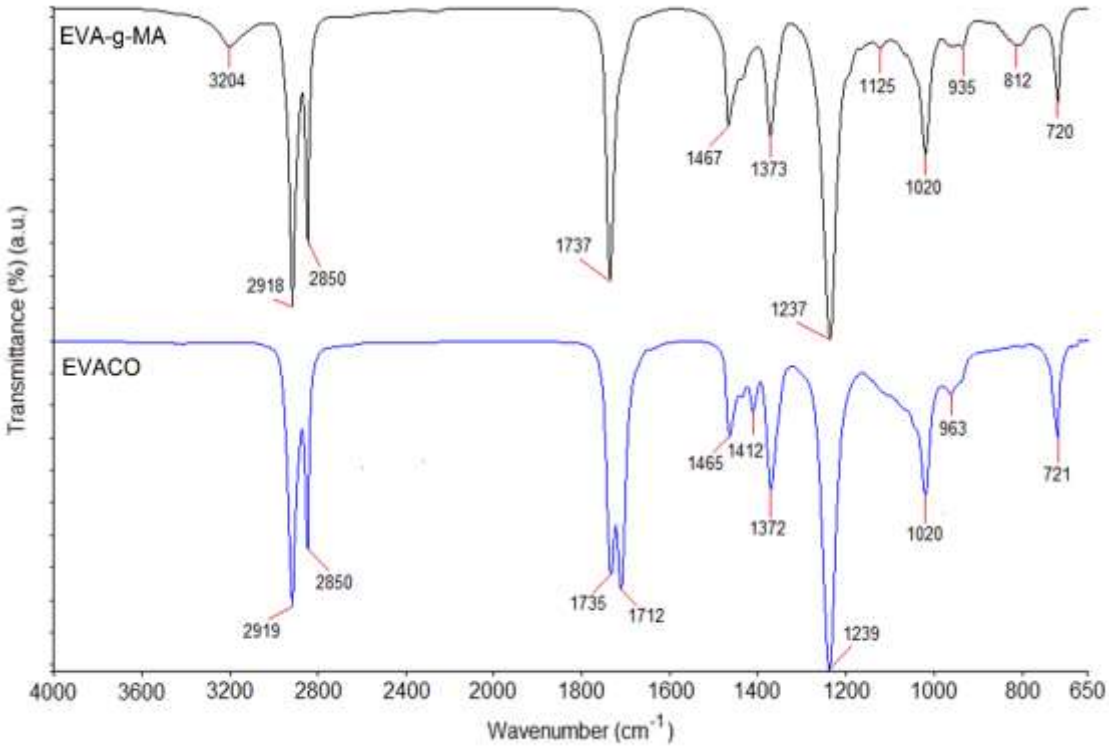

Figure S6. FTIR spectra of EVA-g-MA and EVACO.

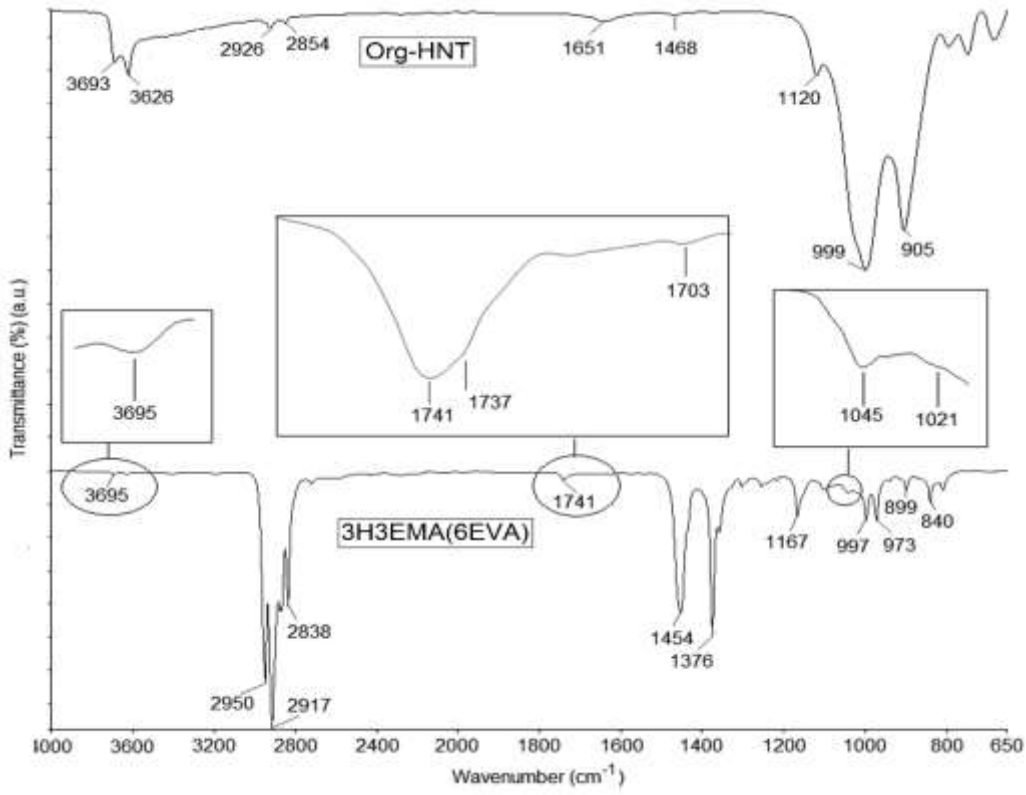

Figure S7. FTIR spectra of Org-HNT and 3H3EMA(6EVA).

DSC analyses of PP, PP blends and nanocomposites

Non-isothermal crystallization temperatures and melting temperatures of PP, PP blends and PP nanocomposites were determined by DSC analyses. Table S1 shows the results of DSC analysis. Figure S8 and Figure S9 show DSC thermograms of crystallization and melting peaks, respectively.

Table S1. The results of DSC analyses for neat PP, PP/EVA blends and composites.

Material	T_m (°C)	X_C (%)	T_c (°C)
PP	**166.69**	**38.38**	**117.16**
PP3EVA	**163.53**	**46.73**	**117.12**
1H3EVA	163.72	48.15	117.28
1H1EMA(2EVA)	164.68	46.12	115.15
1H1ECO(2EVA)	164.84	45.86	117.19
1H1PMA(2EVA)	165.49	44.68	118.94
PP9EVA	**163.81**	**44.93**	**116.60**
3H9EVA	165.11	46.10	116.36
3H3EMA(6EVA)	163.72	46.22	115.43
3H3ECO(6EVA)	163.90	47.17	116.78
3H3PMA(6EVA)	164.59	46.57	118.51
PP15EVA	**164.69**	**44.63**	**116.37**
5H15EVA	165.02	45.96	115.87
5H5EMA(10EVA)	164.83	44.97	115.34
5H5ECO(10EVA)	165.17	46.04	116.31
5H5PMA(10EVA)	164.32	46.92	118.05
PP1H	164.73	46.47	117.72
PP3H	164.68	47.85	120.25
PP5H	164.94	48.65	121.14

According to the results, the crystallization percentages of all materials were higher than pure PP polymer. The percentage of crystallization of polypropylene in PP3EVA blend was found to be 8.35 % higher than that of neat PP (Table S1). This increase can be attributed to the EVA polymer acting as a nucleant for the polypropylene.[14-16] As compared to PP3EVA, PP9EVA and PP15EVA blends containing relatively a higher percentage of EVA, exhibit lower crystallization temperatures but they are still higher than PP (Table S1).

1H3EVA nanocomposite showed a slightly higher percentage of crystallization compared to pure PP3EVA blend. This is due to the fact that silica nanotubes cause heterogeneous nucleation by showing a nucleant effect for the PP matrix.[17] This change in the percentage of crystallization between PP3EVA and 1H3EVA has also been observed in PP9EVA and

3H9EVA and, PP15EVA and 5H15EVA and can be attributed to the reasons mentioned above. In systems using EVA-g-MA, EVACO and PP-g-MA compatibilizers, some differences were observed in the percent crystallization. When 1% Org-HNT was used, it was found that there was a reduction in the percentage of crystallization (Table S1), probably due to the reduced nucleation effect of the nanotubes interacting with these compatibilizers rather than polypropylene. It was reported in the literature that organophilic MMT[18] and layered double hydroxide (LDH) fillers[19] used in PP / EVA systems exhibited similar decreasing nucleant effect due to their interactions via EVA phase.

It is also seen from Table S1 that nanocomposites containing 3% and 5% by weight of Org-HNT and EVACO compatibilizer have higher PP crystallization percentages, probably in accordance with the better distribution of nanotubes in the matrix in those composites (Figure 6-Figure 8, main article). Furthermore, as can be seen from Figure S8, the crystallization peak onset temperatures of nanocomposites is higher than that of neat PP polymer.

Crystallization percentages and crystallization temperatures of PP/Org-HNT binary composites were increased compared to that of neat PP (Table S1 and Figure S10). This result, as mentioned before, can be due to the fact that HNTs act as nucleating agents in heterogeneous nucleation of PP.[20] This effect of HNTs in the nucleation is more evident in the crystallization temperatures of 3% and 5% Org-HNT loaded PP composites (Table S1). On the other hand, when EVA or the compatibilizers with HNT were added to the PP matrix, T_c values were reduced by lowered nucleation effect due to the interaction / encapsulation of the HNTs with these phases.[18-19]

In the composites with PP-g-MA compatibilizer, higher crystallization percentage and crystallization temperature values than pure PP can be based on increasing intermolecular interaction with the carbonyl groups present in this compatibilizer and co-crystallization effect. [21-24]

In terms of melting temperatures, a slight decrease was observed in all the composites compared to pure PP (Table S1). This result can be attributed to heterogeneous nucleation with HNT and elastomer/compatibilizer contributions, which may lead to possible reduction in the size of to the spherulites, and heterogeneous size distribution of spherulites. The possible formation of relatively more and smaller spherulites may be the reason for lower melting temperatures of the composites.[25]

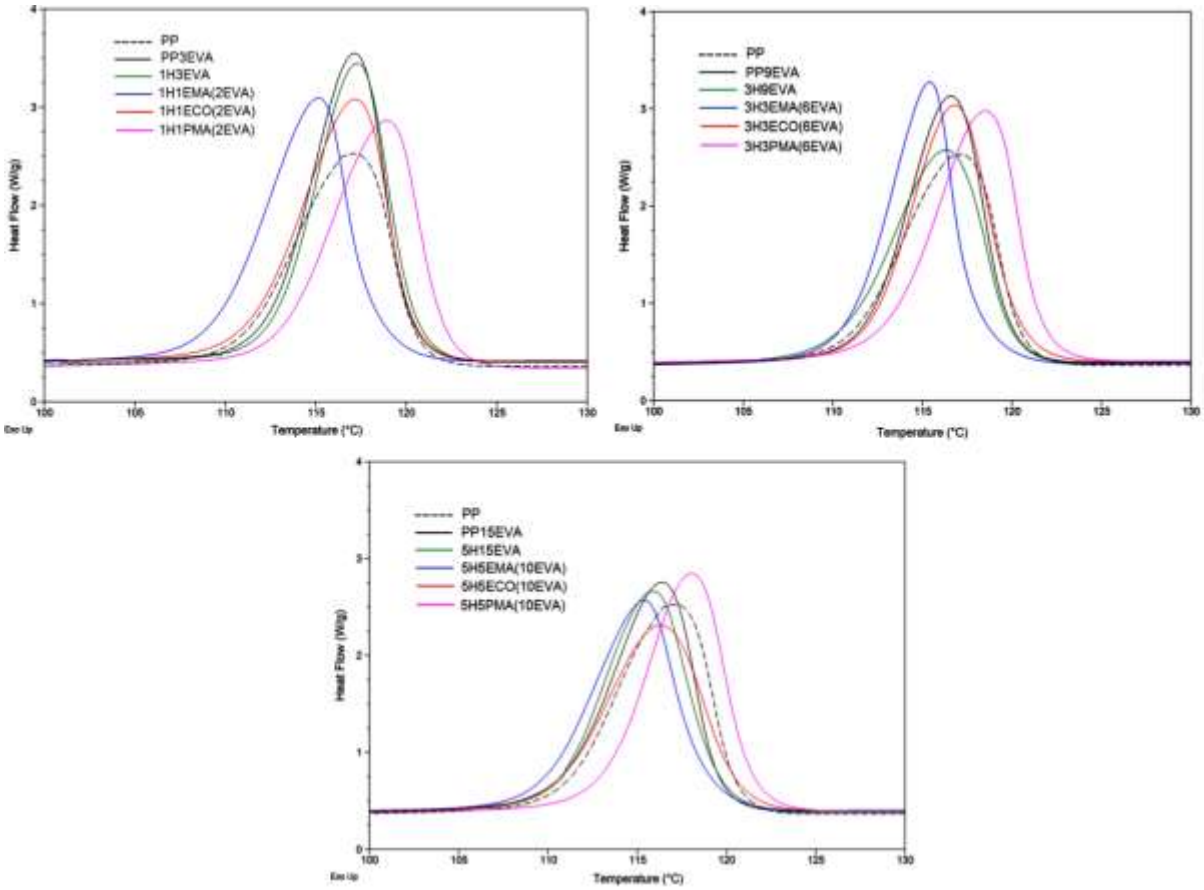

Figure S8. DSC crystallization peaks of PP, PP blends and the nanocomposites containing compatibilizers.

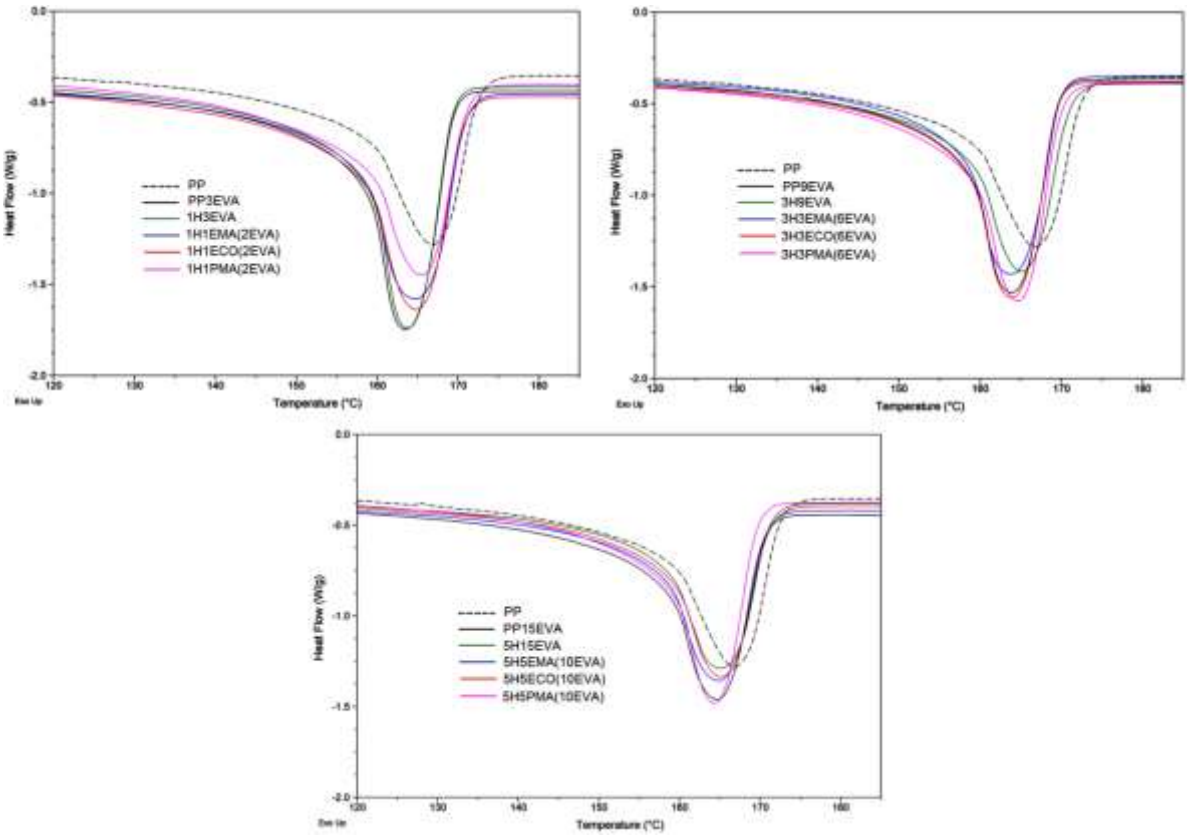

Figure S9. DSC melting peaks of PP, PP blends and the nanocomposites containing compatibilizers.

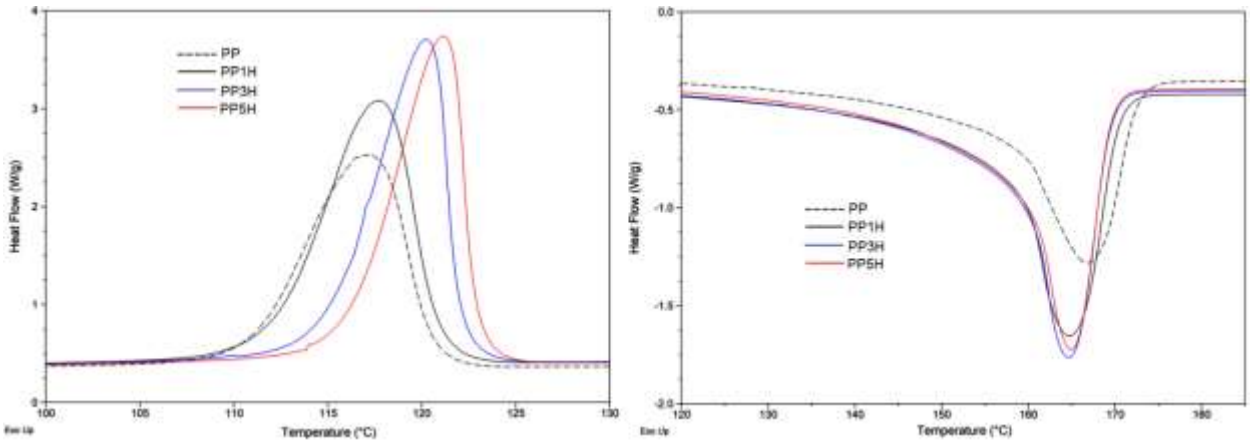

Figure S10. DSC crystallization and melting peaks of PP/HNT binary composites.

SEM images for fractured surfaces of selected samples

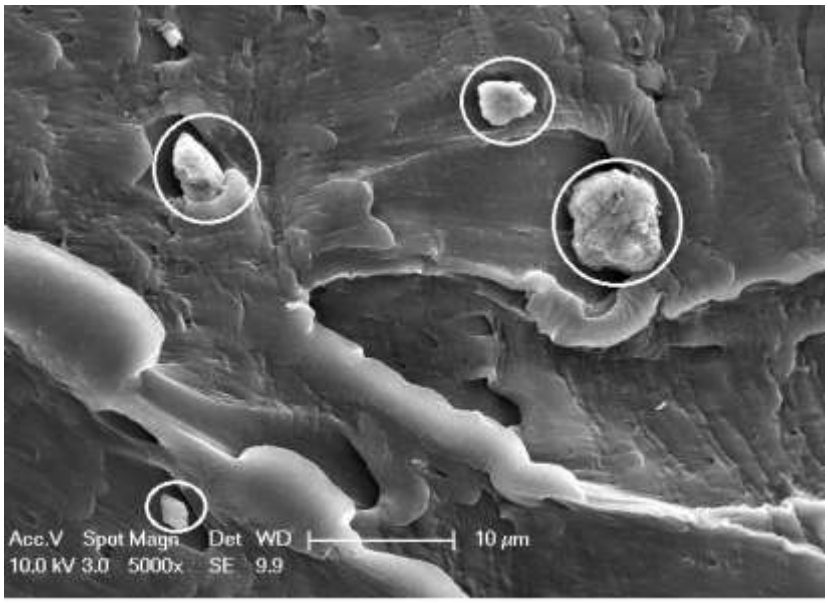

Figure S11. SEM image for the tensile test fractured surface of PP3H.

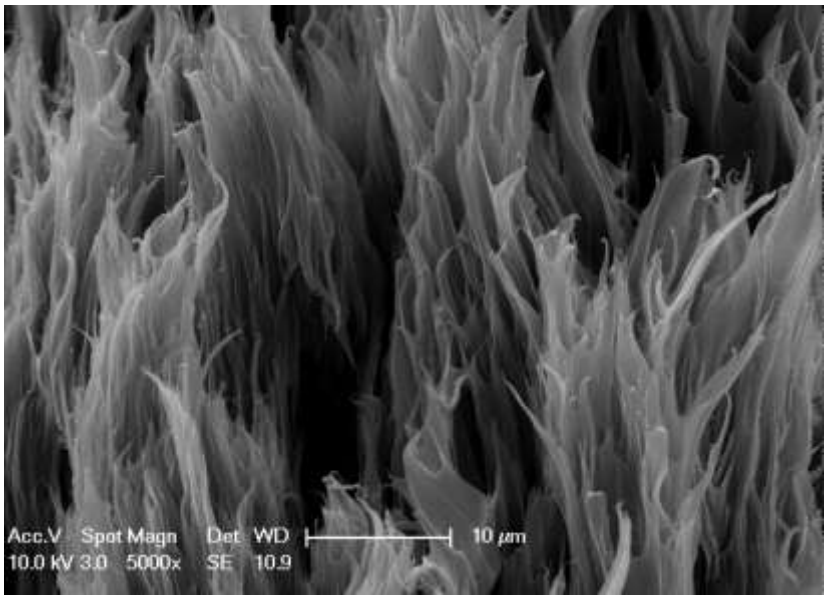

Figure S12. SEM image for the tensile test fractured surface of PP9EVA.

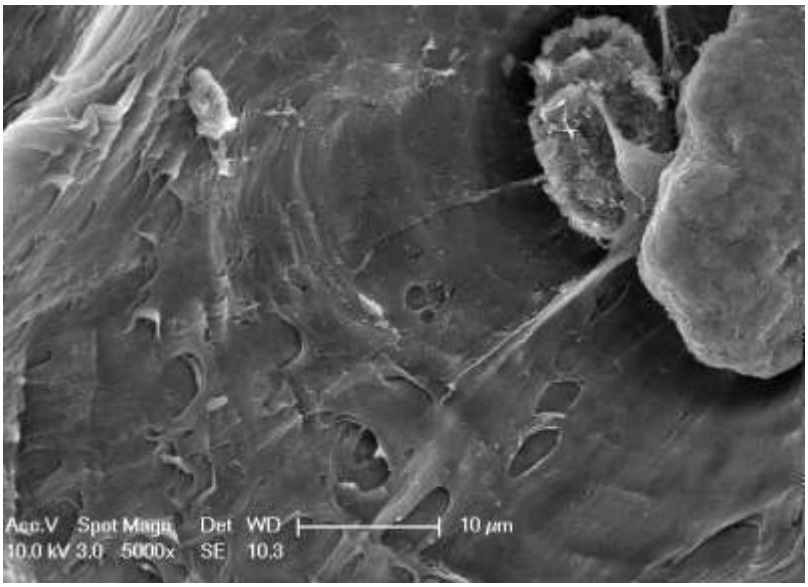

Figure S13. SEM image for the tensile test fractured surface of 3H3PMA(6EVA).

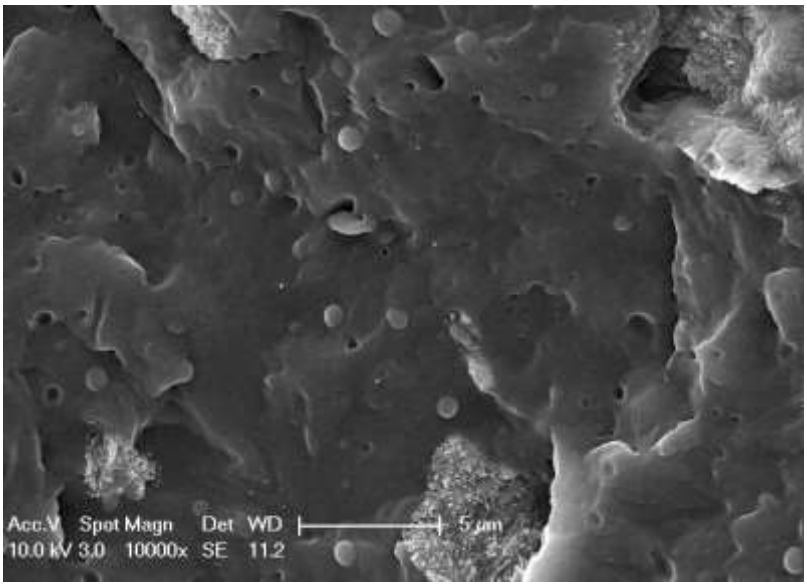

Figure S14. SEM image for the impact fractured surface of 3H3PMA(6EVA).

References

1. de Luna MS and Filippone GJEPJ. Effects of nanoparticles on the morphology of immiscible polymer blends–challenges and opportunities. *Eur Polym J* 2016; 79: 198-218.
2. Tong W, Huang Y, Liu C, et al. The morphology of immiscible PDMS/PIB blends filled with silica nanoparticles under shear flow. *Colloid Polym Sci* 2010; 288: 753-760.
3. Yeniova CE and Yilmazer UJPC. Characteristics of impact modified polystyrene/organoclay nanocomposites. *Polym Compos* 2010; 31: 1853-1861.
4. Guo J, Briggs N, Crossley S, et al. Morphology of polystyrene/poly (methyl methacrylate) blends: effects of carbon nanotubes aspect ratio and surface modification. *AlChE J* 2015; 61: 3500-3510.
5. Dijvejin ZA, Ghaffarkhah A, Sadeghnejad S, et al. Effect of silica nanoparticle size on the mechanical strength and wellbore plugging performance of SPAM/chromium (III) acetate nanocomposite gels. *Polym J* 2019; 51: 693.
6. George G, Selvakumar M, Mahendran A, et al. Structure–property relationship of halloysite nanotubes/ethylene–vinyl acetate–carbon monoxide terpolymer nanocomposites. *J Thermoplast Compos Mater* 2017; 30: 121-140.
7. Arat R and Uyanık N. Surface modification of nanoclays with styrene-maleic anhydride copolymers. *Nat Resour* 2017; 8: 159-171.
8. Wang H, Shi H, Qi M, et al. Structure and thermal performance of poly (styrene-co-maleic anhydride)-g-alkyl alcohol comb-like copolymeric phase change materials. *Thermochim Acta* 2013; 564: 34-38.
9. Rajput RS, Rupainwar D and Singh A. A study on styrene maleic anhydride modification by benzoic acid derivatives and dimethyl sulfoxide. *Int J ChemTech Res* 2009; 1: 915-919.
10. Jamaludin NA, Inuwa IM, Hassan A, et al. Mechanical and thermal properties of SEBS-g-MA compatibilized halloysite nanotubes reinforced polyethylene terephthalate/polycarbonate/nanocomposites. *J Appl Polym Sci* 2015; 132.
11. Pasbakhsh P, Ismail H, Fauzi MA, et al. Influence of maleic anhydride grafted ethylene propylene diene monomer (MAH-g-EPDM) on the properties of EPDM nanocomposites reinforced by halloysite nanotubes. *Polym Test* 2009; 28: 548-559.
12. Bhuvana S and Prabakaran M. Synthesis and characterisation of polyamide/halloysite nanocomposites prepared by solution intercalation method. *Nanosci Nanotechnol* 2014; 4: 44-51.
13. Zhou X, Zhang Q, Wang R, et al. Preparation and performance of bio-based carboxylic elastomer/halloysite nanotubes nanocomposites with strong interfacial interaction. *Compos PT A Appl Sci Manuf* 2017; 102: 253-262.
14. Kakkar D and Maiti S. Effect of flexibility of ethylene vinyl acetate and crystallization of polypropylene on the mechanical properties of i-PP/EVA blends. *J Appl Polym Sci* 2012; 123: 1905-1912.
15. Liu L, Wang Y, Xiang F, et al. Effects of functionalized multiwalled carbon nanotubes on the morphologies and mechanical properties of PP/EVA blend. *J Polym Sci Pol Phys* 2009; 47: 1481-1491.
16. Varghese AM, Rangaraj VM, Mun SC, et al. Effect of Graphene on polypropylene/maleic Anhydride-graft-ethylene–vinyl acetate (PP/EVA-g-MA) blend: mechanical, thermal, morphological, and rheological properties. *Ind Eng Chem Res* 2018; 57: 7834-7845.
17. Wang B and Huang H-X. Effects of halloysite nanotube orientation on crystallization and thermal stability of polypropylene nanocomposites. *Polym Degrad Stabil* 2013; 98: 1601-1608.
18. Goodarzi V, Jafari SH, Khonakdar HA, et al. Nonisothermal crystallization kinetics and determination of surface-folding free energy of PP/EVA/OMMT nanocomposites. *J Polym Sci Pol Phys* 2009; 47: 674-684.

19. Rafiee F, Otadi M, Goodarzi V, et al. Thermal and dynamic mechanical properties of PP/EVA nanocomposites containing organo-modified layered double hydroxides. *Compos Part B-Eng* 2016; 103: 122-130.
20. Kubade P and Tambe P. Influence of surface modification of halloysite nanotubes and its localization in PP phase on mechanical and thermal properties of PP/ABS blends. *Compos Interfaces* 2017; 24: 469-487.
21. Oromiehie A, Ebadi-Dehaghani H and Mirbagheri S. Chemical modification of polypropylene by maleic anhydride: melt grafting, characterization and mechanism. *Int J Chem Eng Appl* 2014; 5: 117.
22. Bogoeva-Gaceva G, Janevski A and Mader E. Nucleation activity of glass fibers towards iPP evaluated by DSC and polarizing light microscopy. *Polymer* 2001; 42: 4409-4416.
23. Menyhárd A, Faludi G and Varga J. β-Crystallisation tendency and structure of polypropylene grafted by maleic anhydride and its blends with isotactic polypropylene. *J Therm Anal Calorim* 2008; 93: 937-945.
24. Devrim YG, Rzaev ZM and Pişkin E. Functionalization of isotactic polypropylene with citraconic anhydride. *Polym Bull* 2007; 59: 447-456.
25. Weeks JJ. Melting temperature and change of lamellar thickness with time for bulk polyethylene. *J Res Natl Bur Stand A* 1963; 67: 441-451.